Applied Thermal Engineering 195 (2021) 117250

Contents lists available at ScienceDirect

Applied Thermal Engineering

journal homepage: www.elsevier.com/locate/apthermeng

Prediction of hydrogen-heavy fuel combustion process with water addition in an adapted low speed two stroke diesel engine: Performance improvement

J. Serrano *, F.J. Jiménez-Espadafor, A. López

Department of Energy Engineering, Seville University, Spain, Camino de los Descubrimientos, s/n, 41092 Sevilla, Spain

ARTICLE INFO

Keywords:
Hydrogen
Water injection
Marine diesel engine
Dual-fuel
Carbon dioxide

ABSTRACT

Despite their high thermal efficiency (>50%), large two-stroke (2 T) diesel engines burning very cheap heavy fuel oil (HFO) produce a high level of carbon dioxide (CO_2). To achieve the low emission levels of greenhouse gases (GHG) that will be imposed by future legislation, the use of hydrogen (H_2) as fuel in 2 T diesel engines is a viable option for reducing or almost eliminate CO_2 emissions. In this work, from experimental data and system modelling, an analysis of dual combustion is carried out considering different strategies to supply H_2 to the engine and for different H_2 fractions in energy basis. Previously, a complete thermodynamic model of a 2 T diesel engine with an innovative scavenging model is developed and validated. The most important drawbacks of this type of engines are controlled in this work using dual combustion and water injection, reducing nitrogen oxides emissions (NOx), self-ignition and combustion knocking. The results show that the developed model matches engine performance data in diesel mode, achieving a higher efficiency and mean effective pressure (MEP) in hydrogen mode of 53% and 14.62 bar respectively.

1. Introduction

The worldwide focus on fossil fuels is increasing due to growing concerns about climate change. For more than 15 years, the authorities have been focused on establishing rules for limiting exhaust gas emissions from two-stroke low-speed diesel engines [1]. This type of engine is used around the world in applications demanding large power output and efficiency, such as ships and electric generation plants [2]. One of the main drawbacks of these engines compared with other types of power plant is the high level of exhaust emissions, which largely comprise CO_2, with smaller quantities of carbon monoxide (CO), oxides of sulphur (SOx) and NOx, partially reacted and non-combusted hydrocarbons (HC) and particulate matter (PM). CO_2 emissions are proportionally related to the consumption of fuel; 1 ton of fuel produces approximately 3 tons of CO_2 [3].

According to the International Maritime Organization (IMO), the shipping industry accounted for 2.1% of global GHG emissions in 2014, due to the burning of fossil fuels as the primary means of propulsion [4], and approximately 13% of global NO_x emissions [5]. The IMO has adopted a strategy to reduce the emission of GHG from global shipping by at least 50% by 2050 [6]. Taking into account the high lifetime of this type of engine, low-speed two-stroke diesel engines and the vessels require changes to meet the challenges ahead.

Several methods are being developed in order to comply with the new restrictions on GHG emissions, such as engine improvements, exhaust gas recirculation (EGR), two-stage turbocharging, selective catalytic reduction (SCR), dual-fuel engines, alternative fuels, batteries and FC [7,8]. In recent years, battery-electric propulsion has successfully been applied for short-sea ferries. Within the field of large ocean-going vessels within the traditional domain of the 2 T diesel engine, short-sea Ro-Ro shipping seems to be the only area where battery-electric propulsion constitutes an alternative that is practically feasible weight- and volume-wise at the current stage of development of battery technology [6,9]. A 2 T engine operating on carbon–neutral fuels seems a more attractive solution for large ocean-going vessels to become carbon neutral due to the cost, weight, volume and expected useful life of batteries.

Alternatively, FC systems provide an efficient way to generate electricity with few emissions [10]. Currently available FC systems are significantly more expensive than conventional generators, but it is expected that system prices can be reduced to levels where the higher investment cost is justified by the advantages. In this regard, H_2 is considered as an alternative fuel for power generation especially in the

* Corresponding author.
E-mail address: jserrano9@us.es (J. Serrano).

https://doi.org/10.1016/j.applthermaleng.2021.117250
Received 2 October 2020; Received in revised form 7 April 2021; Accepted 15 June 2021
Available online 18 June 2021

Nomenclature

2 T	Two-stroke
A_1	Released energy during the premixed phase
A_2	Released energy during the diffusion phase
A_a	Area of the intake ports
A^{adm}	Side area of each region
A^{esc}	Exhaust area of each region
BDC	Bottom dead centre
C_1	Shape factor
C_2	Shape factor
CI	Compression ignition engine
c_{ld}	Constant heat capacity of diesel in liquid state
c_p	Specific heat at constant pressure
c_v	Specific heat at constant volume
D_p	Piston diameter
EGR	Exhaust gas recirculation
EVC	Exhaust valve closing
EVO	Exhaust valve opening
FC	Fuel cell
Fr	Energy fraction of hydrogen
G	Flow
g_c	Corrected volume flow
GHG	Greenhouse gas
h	Specific enthalpy
H_a	Height of the intake ports
H_i	Height of the bottom side
H_p	Piston position
HFO	Heavy fuel oil
HRR	Heat release rate
IC	Intake ports closing
IMO	International Maritime Organization
IO	Intake ports opening
J	Piston rod and piston length
l_m	Longitudinal shaft
m_1	Shape factor
m_2	Shape factor
m	Mass
MEP	Mean effective pressure
n	Moles
N	Total number of species
N_c	Corrected revolutions
p	Pressure
PHRR	Parametric heat release rate
PM	Particulate matter
Q	Heat transfer
R	Specific gas constant
RPM	Revolutions per minute
SCR	Selective catalytic reduction
T	Temperature
TDC	Top dead centre
u	Internal energy
U	Total internal energy
V	Volume
V_c	Swept volume
$\dot{W}$	Power
WI	Water injection
x	Species
Z	Total number of regions

Greek symbols

β	Shape parameter of the turbine
θ	Crank angle
θ_{c1}	Angle corresponding to the maximum HRR in the premixed phase
θ_{c2}	Angle corresponding to the maximum HRR in the diffusion phase
τ	Mass ratio between diesel and hydrogen
ϕ	Flow between regions
π	Compression ratio
η	Efficiency
μ	Mass ratio between water and hydrogen
υ	Angle between the connecting rod and the longitudinal shaft

Subscripts

cmb	Relative to the combustion
cmp	Relative to the compressor
d	Relative to the diesel
evp	Relative to the evaporation
h_2	Relative to the hydrogen
inj	Relative to the injection
i	Relative to the region
j	Relative to the species
k	Relative to the plenums
ld	Relative to the liquid diesel
r	Relative to the combustion phase
ref	Relative to the reference conditions
trb	Relative to the turbine
wll	Relative to the wall

transportation sector, such as maritime [11]. Some of the characteristics that make H_2 attractive as an alternative fuel are: high heating value, wide flammability range, high flame speed, zero carbon content, high diffusivity, low minimum ignition energy and that it can be produced from renewable energy and can be stored easily [12,13].

On the contrary, H_2 cannot be directly used in compression ignition engines due to its high self-ignition temperature, which would require a prohibitively high compression ratio and/or heating of the intake air, reducing the volumetric efficiency and therefore the engine power. Although H_2 can be burnt in dual-fuel mode using diesel fuel as the ignition source [14] or with spark plugs [15], several major problems with hydrogen as fuel are yet to be resolved, including combustion knock and high NOx emissions [16,17].

Regarding co-combustion studies developed in naturally aspirated heavy-duty engines, it has been shown a reduction in exhaust emissions of NOx and PM at low H_2 levels; however, at higher H_2 levels, an increase in both exhaust NOx and PM emissions has been observed [18,19]. NOx emissions were speculated to increase due to higher in-cylinder gas temperatures resulting from H_2 combustion, while PM emissions increased due to displacement of intake O_2 by H_2 [18]. Some studies have attempted to reduce the NOx and PM emission levels by utilizing EGR in heavy-duty engines [20]. The effect of EGR with dual H_2–diesel co-combustion was to achieve simultaneous reductions in smoke and NOx emissions [20,21]. Other studies have investigated the effect of an elevated intake air temperature on an engine operating on H_2 and diesel as fuels, and a considerable reduction in exhaust emissions was achieved (41% NOx and 30% PM emissions reduction), although the authors observed no significant impact of intake air temperature on engine performance [22]. Studies with water injection (WI) that have been carried out in current diesel engine technology show better NOx and PM reductions than those achieved with the use of EGR [23]. In addition, WI is able to prevent the self-ignition and combustion knocking in dual combustion mode [24,25].

The aim of this work is to study the feasibility of using hydrogen in

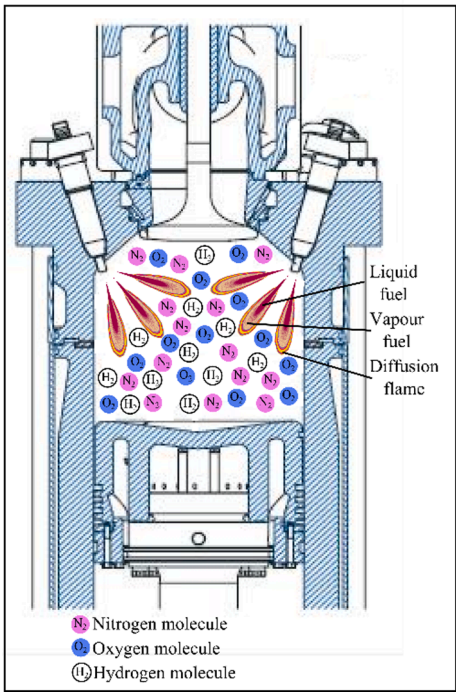

Fig. 1. Scheme of dual combustion in the combustion chamber of a large 2 T engine with two diesel injectors and one exhaust valve.

Table 1
MAN B&W 10L67GBE specifications.

Type	Two-stroke low-speed diesel engine
Stroke	1700 mm
Bore	670 mm
Cylinder displacement	599.361 cm^3
Connecting rod length	2549 mm
Connecting rod length/ crank length ratio	2.9988
Maximum power	16 MW
Nominal speed	125 rpm
Firing order	1-9-4-6-3-10-2-7-5-8
Engine cooling	Water-cooled
Turbocharger cooling	Water–air heat exchanger
Fuel	Heavy fuel oil with sulphur less than 1%.
Specific HFO consumption at maximum continuous ratio (MCR)	195.9 g/kW h
Diagram of distribution	Intake opening (IO): 48° before BDCIntake closing (IC) : 48° after BDCExhaust valve opening (EVO) : 65° before BDCExhaust valve closing (EVC) : 92° after BDC Start of fuel oil injection: 5° before TDC

low-speed 2 T diesel engines, since currently there is not any internal combustion engine like this -used for ship propulsion and power plants- operating with hydrogen. However, natural gas (GN) is being used to replace heavy fuel oil, mainly because its low CO2/MJ ratio, and also because can be mixed with small hydrogen proportion to improve GN combustion. It is worth to mention that nowadays gas turbines are being tested on 100% hydrogen in power plants such as the 12 MW 'Hyperflower' plant in France or the plant of 10 MW in Port Lincoln (Australia).

This paper presents the development of a 2 T diesel engine model, validated with engine performance data, and its adaptation to dual combustion mode (H_2–diesel) with water injection. The engine is simulated through a mixed thermodynamic model that includes compressor and turbine operation maps and the generation of a piston performance map. This mixed model is a combination of an innovative scavenging multi-zone model that does not require an external law, and a zero-dimensional model for diesel injection and HFO and hydrogen combustion.

In this work, the study is focused on the effects of the addition of H_2 combined with WI on the in-cylinder pressure and temperature, the efficiency and MEP under various engine loads, water and H_2 fractions. Two ways of supplying hydrogen to the engine will also be studied; through the intake ports during air induction and by injection during the compression stroke. Fig. 1 shows a scheme of dual combustion inside the combustion chamber of a large 2 T engine with two diesel injectors and one exhaust valve.

2. Methodology

2.1. Engine description

The model has been developed for the diesel engine MAN B&W 10L67GBE, the main characteristics of which are shown in Table 1; a 2 T low-speed diesel engine with in-line 10 cylinders. Each cylinder has lateral intake ports and a single exhaust valve in the cylinder head.

This low-speed engine is characterised by operating in the two-stroke diesel cycle, uniflow scavenging, a single exhaust valve in the cylinder head, two turbochargers with charge cooler and flat piston geometry. Fig. 2 shows a longitudinal section of this type of engine.

2.2. Engine model

This section gives a description of the main hypotheses on which the model is based and the full integration of the thermodynamic model, that is, the combination of the compressor and turbine operation maps with the engine sub-models that it is shown in Fig. 3.

The engine is formed as is shown in Fig. 4 by:

- Two compressors that take the air from atmospheric conditions, and increase the air pressure and density feeding the plenum, having passed the air previously through an air–water cooler.
- The engine block with 10 cylinders where each cylinder takes the compressed air from the plenum and expels the exhaust gases to one of the two exhaust manifold, one for each group of five cylinders.
- Two turbines, one for each exhaust manifold, through which the exhaust gases expand and move their respective compressors. A diffuser is at the exit of each turbine to maximise expansion.

For any fuel flow, the two-stroke low-speed engine model provides:

- Thermodynamic state of gases at combustion chamber.
- Operating point of compressors and turbines.
- Thermodynamic state of air and exhaust gases at plenum and exhaust manifold.

To generate the cylinder operation map, a mixed model is developed where a combination of a multi-zone model for scavenging and a zero-dimensional model for hydrogen and HFO combustion with the possibility of water addition are used. The engine model involves solving mass and energy balances with geometric equations.

The novelty regarding the development of the thermodynamic model of the engine is the use of an innovative multi-zone scavenging model that does not require an external law to define the flow inside the combustion chamber. The scavenging model has been introduced because in 2 T engines scavenging is critical from the point of view of engine performance and therefore it has to be considered.

The volume of the combustion chamber is divided into several regions in the multi-zone scavenging model that applies when the inlet ports or exhaust valve are open. In the zero-dimensional combustion model, only one region is considered, where the pressure, temperature

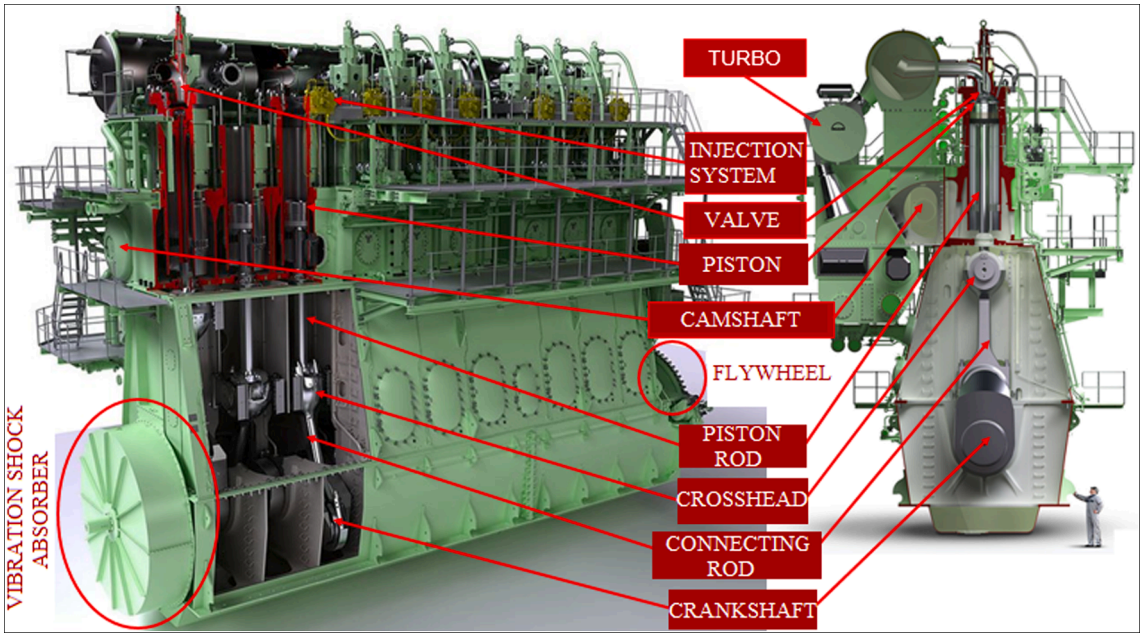

Fig. 2. MAN B&W diesel's MC-GI low-speed engine [26].

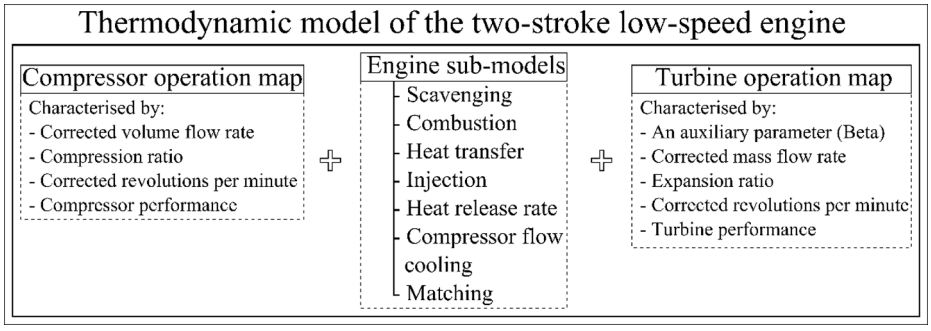

Fig. 3. Thermodynamic model scheme of the two-stroke low-speed diesel engine.

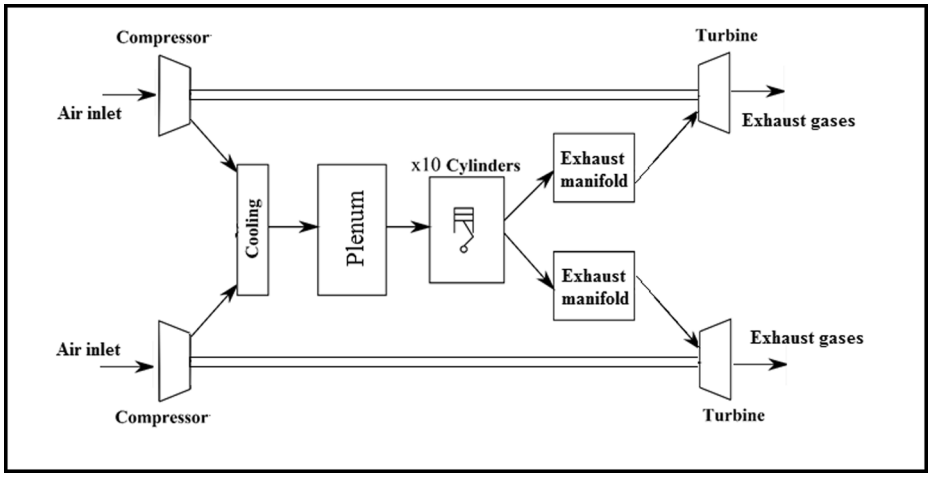

Fig. 4. Complete engine diagram.

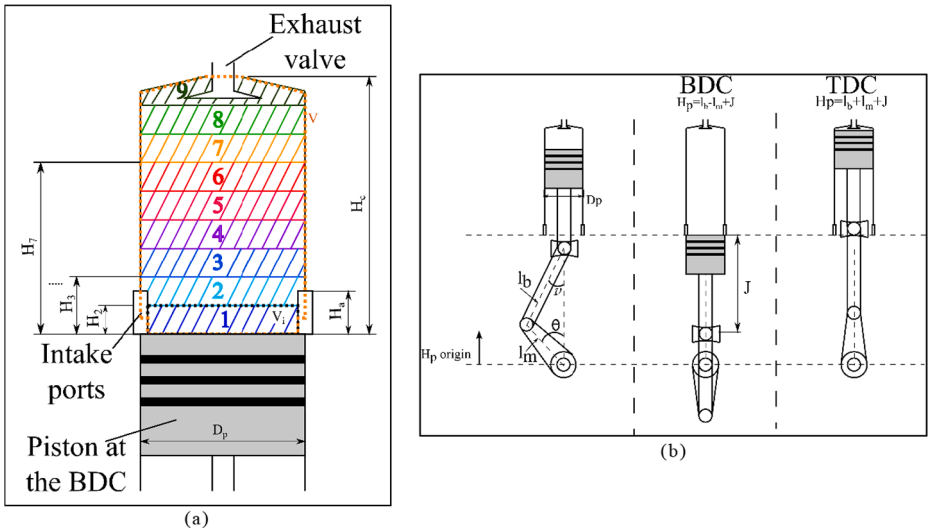

Fig. 5. (a) Regions for scavenging model and (b) kinematic chain of the 2 T engine.

and chemical species are homogeneous. Fig. 5(a) shows the geometrical boundary conditions for the scavenging model and Fig. 5(b) shows the kinematic chain involved in the 2 T engine model.

2.2.1. Scavenging model

During the scavenging phase, fresh air enters via the intake ports located at the bottom of the cylinder and the exhaust gases along with a small part of the fresh air leave the chamber through the exhaust valve located at the top of the cylinder. The developed scavenging model is an innovative multi-zone model that does not require an external law to define the sweep inside the combustion chamber.

To model the scavenging process, often two limited ideal models are used [27] although none of them have been used in this case:

- The perfect displacement model. It is assumed that burned gases are pushed out by the fresh gases without any mixing.
- The complete mixing model. Fresh mixture entering mixes instantaneously and uniformly with the burned gases.

In the proposed scavenging model, the volume of the combustion chamber is divided into regions as is shown in Fig. 5(a). The intake flow mixes instantaneously due to the small size of the slices in this region. Between consecutive slices there is a mass flow that adjusts to their volume change (due to the piston movements) and to the exchanges with the outside (through the intake ports and the exhaust valve). This flow between slices is the cause of displacement.

Fig. 5(a) illustrates a representative scheme of the number of regions. The selection of the number of zones has required an analysis of the number of volumes into which to divide the combustion chamber to reach the adequate number of regions; as a result the optimal number of regions is 9. To set this number, the following criterion has been followed:

1) The number of regions is considered such that the evolution of the temperature in the last zone (zone 9 in Fig. 5(a), the one in contact with the exhaust valve) converges.
2) The number of regions is the minimum that guarantees that the conditions of the turbine inlet flow are independent of the number of regions. Saying in a different way, increasing the number of zones does not change flow conditions at turbine inlet.

The following hypotheses have been taken into account to develop the scavenging model:

- The pressure is uniform throughout the cylinder.
- Each region has its own temperature, mass and composition.
- Heat transfer with cylinder walls is neglected. This is because during the scavenging phase there are no large temperature gradients between cylinder walls and gases.

The equations that define the scavenging model are described in the following sub-sections.

2.2.1.1. Geometric equations. As we have already mentioned, the distinction in regions will be made for the scavenging model. In the case of the combustion model, the entire volume of the combustion chamber corresponds to a single region. These equations provide: the position of the piston, the total volume of the combustion chamber, the area of the intake ports and the area of the exhaust valve at each crank angleθ. These equations are based on the connecting rod - crank mechanism and allow us to define:

$$V_i(\theta) = \frac{\pi D_p^2}{4M}\left(H_c - H_p(\theta)\right) \text{ [Volume of each region]} \quad (1)$$

$$H_i(\theta) = H_p(\theta)\frac{i-1}{M} \text{ [Position of the bottom side of each region]} \quad (2)$$

2.2.1.2. Energy and mass balance. The thermodynamic properties of each region are described as follows. Each region "i" is defined by: the temperature T_i; the mass m_{ij} of each species $j = 1, \ldots, N$ and the volume V_i.

A set of differential equations are solved to calculate the thermodynamic states in each region "i". Included in these is an energy balance, a mass balance, an equation of state, heat losses and heat release correlations. The general energy balance is formulated as follows:

$$\frac{dU}{dt} = \frac{dW}{dt} + \frac{dQ_{cmb}}{dt} + \frac{dQ_{wll}}{dt} + \dot{m}_i \cdot \dot{h}_i - \dot{m}_0 \cdot \dot{h}_0 \quad (3)$$

The change of mass of each species in each region is due to the flow that it exchanges with the lower region, with the upper one, with the intake ports, the exhaust valve and during the combustion, the change of mass of each species is due to the fuel injection and the combustion itself:

$$\frac{dm_j}{d\theta} = \frac{\partial m_{cmb,j}}{\partial x_{cmb}} \cdot \frac{dx_{cmb}(\theta)}{d\theta} + \overline{m}_j \cdot \frac{dx_{iny,j}(\theta)}{d\theta} \quad (4)$$

The differential form of the general energy balance is:

$$\sum_j m_j c_{vj}(T)\cdot\frac{dT}{d\theta} = -p\cdot\frac{dV(\theta)}{d\theta} - \sum_j \frac{dm_j}{d\theta}u_j(T) + \frac{dQ_{cmb}(\theta)}{d\theta} + \frac{dQ_{wll}(\theta)}{d\theta} + \frac{dm_{iny,d}(\theta)}{d\theta}\left[h_{ld}\left(T_{iny,d}\right) + R_d\cdot T_{ref}\right] + \frac{dm_d}{d\theta}\left[c_{vd}\left(T_{ref} - T_{evp}\right) + L_{evp} + c_{ld}\left(T_{evp} - T_{ref}\right)\right] \quad (5)$$

Its integration allows the cylinder pressure, temperature and mass of each species in each region to be determined, as well as the flows between regions and the intake and exhaust flows.

2.2.1.3. Flow balances. To define the flow balances in each region, it must be taken into account that there are two types of flow. There is the flow between consecutive slices and the flow of the slices into contact with the intake ports and the exhaust valve.

First, the flow between consecutive regions is analysed, where ϕ_i defines the flow from the region i to $i+1$ (positive) or the flow between the region $i+1$ to i (negative).

$$\phi_{ij} = x_{ij}^{\pm}\cdot\phi_i, x_{ij}^{\pm} = \begin{cases} x_{ij} & if\ \phi_i > 0 \\ x_{i+1j} & if\ \phi_i < 0 \end{cases} \quad (6)$$

$$h_i^{\pm} = \begin{cases} h_i & if\ \phi_i > 0 \\ h_{i+1} & if\ \phi_i < 0 \end{cases} \quad (7)$$

The result of these flows at each angle is obtained from the system of linear equations resulting from applying the mass, energy and gas balance equations to each region. The external flow (φ_{ij}^k), due to the contact with the intake ports or the exhaust valve, is modelled on a discharge through a convergent nozzle that connects each region i with the respective plenum k.

$$\varphi_{ij}^k = \begin{cases} \pm x_{ij}^k C_D^k A_i^k \dfrac{p_0^k}{\omega\sqrt{R^k T_0^k}}\gamma^k\left(\dfrac{2}{\gamma^k+1}\right)^{\frac{\gamma^k+1}{2(\gamma^k-1)}} & if\ \dfrac{p_1^k}{p_0^k} < \left(\dfrac{2}{\gamma^k+1}\right)^{\frac{\gamma^k}{\gamma^k+1}} \\ \pm x_{ij}^k C_D^k A_i^k \dfrac{p_0^k}{\omega\sqrt{R^k T_0^k}}\left(\dfrac{p_1^k}{p_0^k}\right)^{1/\gamma^k}\sqrt{\dfrac{2\gamma^k}{\gamma^k-1}\left[1-\left(\dfrac{p_1^k}{p_0^k}\right)^{\frac{\gamma^k-1}{\gamma^k}}\right]} & if\ \dfrac{p_1^k}{p_0^k} < \left(\dfrac{2}{\gamma^k+1}\right)^{\frac{\gamma^k}{\gamma^k+1}} \end{cases} \quad (8)$$

If the plenum pressure is higher than the pressure of the region i, the flow has a positive sign (the flow enters into the combustion chamber). The variables p_0^k, T_0^k, R^k and γ^k are the conditions of the plenum k and the in-cylinder pressure is p_1^k.

If the plenum pressure is lower than the pressure of the region i, the flow has a negative sign (the flow leaves the cylinder). The variables p_0^k, T_0^k, R^k and γ^k are the conditions of the region i and the plenum k pressure is p_1^k.

2.2.2. Combustion model

The scavenging phase occurs while the intake ports are open. During this phase air, water and H_2 mix in the engine plenum. For the case of H_2 injection presented in Section 3, only air and water are mixed.

When the exhaust valve closes, 92° after BDC, the compression phase begins. Subsequently, HFO is injected 5° before TDC and combustion of both fuels develops after a small combustion delay. When the exhaust valve opens at 65° before BDC, the scavenging phase starts again.

The following hypotheses have been taken into account in the combustion model:

- The gas is uniformly distributed throughout the combustion chamber volume with homogeneous pressure, temperature and composition. When the scavenging process ends, the mass of each species in each region is known. The total mass of a species contained in the cylinder will be the sum of the masses of that species in each of the regions. In this way the mass of each species contained in the cylinder will be known when it is passed from the multi-zone model to the mono-zone model. To determine the in-cylinder temperature at the beginning of the combustion process the ideal gas equation is applied, since the total mass, the pressure and the volume are known.
- HFO is considered to be injected in a liquid state and evaporates instantly, which is compatible with the very low engine speed. The evaporation process is taken into account when calculating the internal energy of HFO.
- The heat capacity of HFO is constant both in the liquid phase and in the gas phase.
- The combustion chamber is considered completely rigid and non-deformable.
- Heat losses are considered during combustion due to high temperature gradients between the gases and cylinder wall.
- Heat losses are not considered during scavenging due to the very low temperature gradients between the gases and cylinder wall.
- The combustion rate per each HFO-H_2 proportion and water fraction is given by a function of the angle of rotation of the crankshaft.

The resolution of the combustion model implies the resolution of the geometry equations, the thermodynamic properties equations, the mass balance, the ideal gas equation and the energy balance such as those described in the scavenging model section (considering a single area) together with the heat transfer model, the fuel injection model and the heat release model.

2.2.3. Heat transfer model

The heat transfer to the combustion chamber walls is essentially governed by convection, since gas radiation to the walls can be neglected under these conditions [28].

In the present model, the Woschni correlation is used to calculate the heat transfer coefficient. The expression used for the heat transfer coefficient is [27]:

$$dQ_{wll} = -h_{wll}A_{wll}(T - Twll) \quad (9)$$

$$h_{wll} = 3.26D_p^{-0.2}\left(\frac{p}{1000}\right)^{0.8}T^{-0.55}\left[2l_m\omega_{eng}C_1 + \frac{V_c T_r}{p_r V_r}(p - p_r)C_2\right] \quad (10)$$

where

- $V_c = \frac{\pi}{4}D_p^2\cdot 2l_m$ is the swept volume.
- p_r, T_r and V_r the pressure, the temperature and the volume at the beginning of the combustion phase.
- $C_1 = 2.28$ and $C_2 = 0$ during the compression.
- $C_1 = 2.28$ and $C_2 = 0$ during the combustion.

2.2.4. Fuel injection model

The fuel injection has an important effect on the mass balance, gas

Table 2
Selected operating points to study the dual-fuel mode.

Rated power (%)	Energy fraction of H_2 (Fr)	$\tau = H_2$ mass/(diesel mass + H_2 mass)	$\mu = H_2O$ mass/ H_2 mass
100-80-60	0	0	0
	0.25	0.1071	0
	0.50	0.2647	17.78
	0.80	0.5902	32.00

composition and energy balance [29]. Diesel is injected at a constant rate between an injection start angle $\theta_{iny,0}$and end of injection$\theta_{iny,f}$, so that the mass injected as a function of the stroke angle is:

$$\frac{dm_{iny,d}}{d\theta} = \overline{m}_d \frac{\theta - \theta_{iny,0}}{\theta_{iny,f} - \theta_{iny,0}}, \theta_{iny,0} < \theta < \theta_{iny,f} \tag{11}$$

where

$$\frac{dx_{iny,j}(\theta)}{d\theta} = \begin{cases} \dfrac{\theta - \theta_{iny,0}}{\theta_{iny,f} - \theta_{iny,0}}, \theta_{iny,0} < \theta < \theta_{iny,f}, & j = diesel \\ 0, & j \neq diesel \end{cases} \tag{12}$$

The mass variation due to the injection can be expressed for all species:

$$\frac{\mathrm{dm_{iny,j}}}{\mathrm{d}\theta} = \overline{\mathrm{m}}_{\mathrm{j}} \frac{\mathrm{dx_{iny,j}}(\theta)}{\mathrm{d}\theta} \tag{13}$$

2.2.5. Heat release rate

The heat release rate (HRR), $\frac{dx_{cmb}}{d\theta}$, measures the rate of progress of the combustion reaction as a function of the crank angle, so the mass of diesel and H_2 that is burned instantaneously is expressed as follows:

$$\frac{dm_{cmb,d}}{d\theta} = -\frac{dx_{cmb}}{d\theta} \cdot \overline{m}_d, \frac{dm_{cmb,H_2}}{d\theta} = -\frac{dx_{cmb}}{d\theta} \cdot \overline{m}_{H_2} \tag{14}$$

where $\overline{m}_d$ is the HFO mass injected per cycle and $\overline{m}_{h2}$ is the H_2 mass existing in the combustion chamber at the beginning of the combustion phase. The change in mass due to combustion can be expressed as:

$$\frac{dm_{cmb,j}}{d\theta} = \frac{\partial m_{cmb,j}}{\partial x_{cmb}} \cdot \frac{dx_{cmb}(\theta)}{d\theta} \tag{15}$$

where j refers to hydrogen and HFO. The heat of combustion is proportional to the heating value of the HFO (Q_d) and H_2 (Q_{H2}), and the mass of both species.

$$dQ_{cmb} = \left(\overline{m}_d Q_d + \overline{m}_{h2} Q_{h2}\right) \frac{dx_{cmb}(\theta)}{d\theta} \tag{16}$$

In other to characterise the HRR, a double Wiebe model has been selected. In the case of a strong premixed combustion phase, as in direct injection engines, a single Wiebe function is not suitable for modelling the heat release characteristics; for a more accurate simulation of the HRR characteristics in diesel engines a combination of two Wiebe functions is more appropriate. Despite its introduction more than 50 years ago, the Wiebe function as a burn fraction or burn rate (both time- and CA-resolved) is widely used. This is because of its simplicity and versatility as demonstrated by its many forms and numerous applications. It is widely used in engine research as a single-function, double-function, or multiple-function prescribed combustion model for investigating a wide variety of engine processes. The parameterisation of this model is based on the Ghojel structure, the first double-Wiebe model devised for the prediction of heat release in direct injection diesel engines. From this double Wiebe model, the six parameters have been set which it has allowed the characterization of the premixed and diffusion combustion phases. These are given by the first and second adding up of the following equations:

$$x_{cmb}(\theta) = +A_1 \cdot \left[1 - e^{-\frac{m_1}{m_1+1}\left(\frac{\theta-\theta_0}{\theta_{c1}}\right)^{m_1+1}}\right] + A_2 \cdot \left[1 - e^{-\frac{m_2}{m_2+1}\left(\frac{\theta-\theta_0}{\theta_2}\right)^{m+1}}\right] \tag{17}$$

$$\frac{dx_{cmb}(\theta)}{d\theta} = +\frac{m_1 A_1}{(m_1+1)\theta_{c1}} e^{-\frac{m_1}{m_1+1}\left(\frac{\theta}{\theta_{c1}}\right)^{m_1+1}} + \frac{m_2 A_2}{(m_2+1)\theta_{c2}} e^{-\frac{m_2}{m_2+1}\left(\frac{\theta}{\theta_{c2}}\right)^{m_2+1}} \tag{18}$$

It is applicable if$\theta > \theta_0$.
The parameters to define the HRR are:

- θ_0 is the starting angle of the combustion phase in relation to the TDC.
- A_1 and A_2 are the energies released during the premixed and diffusion phases, respectively.
- θ_{c1} and θ_{c2} are the angles corresponding to the maximum HRR in the premixed and diffusion phases, respectively.
- m_1 and m_2 are shape factors.

The HRR parameters have been obtained from an experimental previous study by the authors, carried out in a conventional diesel engine for different operation modes with an experimental set close to 200 [24,25]. These HRR parameters are dimensionless and depend on the crank angle. The analysis of error in the experimental work can be consulted in Table 2 of the references [24] and [25]. The novelty regarding the combustion model is the incorporation of these parameterized heat release rates.

In addition to considering the double function of Wiebe, two other alternatives were studied: 1) the Vibe Substitute Heat Release Rate and 2) the Polygon-Hyperbola Substitute Heat Release Rate model. The best results were obtained with the double-Wiebe model and for this reason these previous analyses have not been included in this work.

2.2.6. Compressor flow cooling

Fig. 7 shows the heat exchanger between the compressed air at T_1 and the cooling water (T^{rf}). The outlet temperature of the cooling is

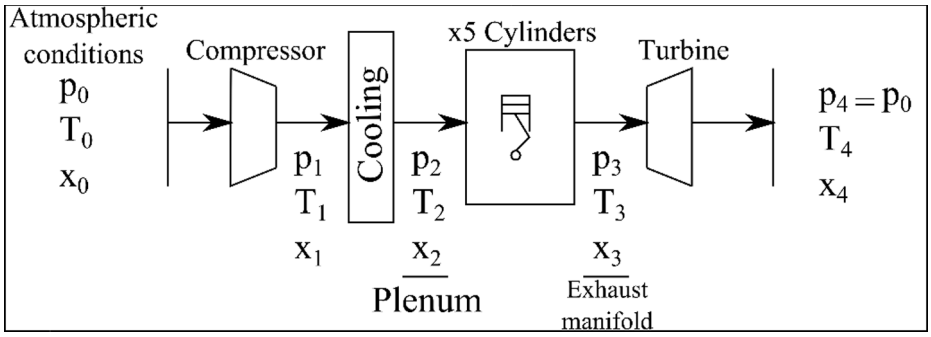

Fig. 6. Simplified engine diagram.

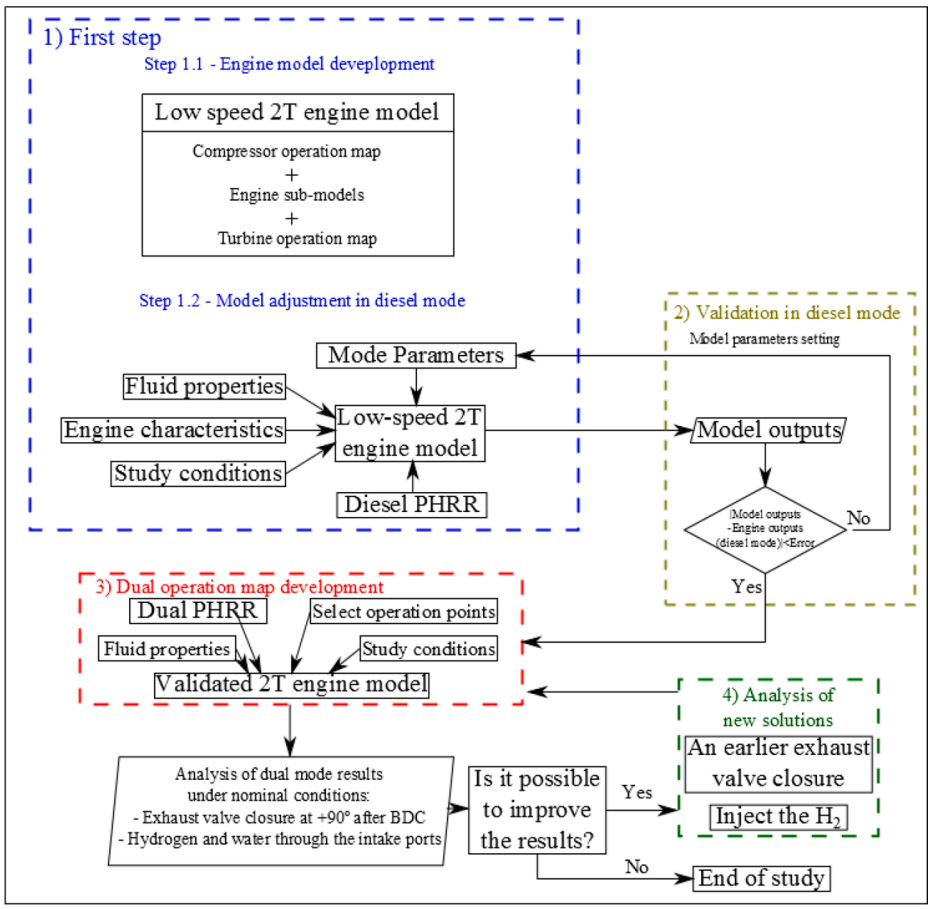

Fig. 7. Diagram of the 2 T engine study.

calculated by a cooling efficiency (η^{rf}):

$$T_{outlet} = T_1 + \eta^{rf}\left(T^{rf} - T_1\right) \tag{19}$$

2.2.7. Matching

When the engine is balanced, it can be assumed that:

- The ten cylinders work under the same conditions.
- Both compressors work under the same conditions, each of them with half of the total engine air flow.
- Both exhaust manifolds are under the same conditions.
- Both turbines work under the same conditions, each of them receiving half of the total engine exhaust flow.

The engine diagram can be represented as shown in Fig. 6.

The different components of the engine can be characterised as follows:

2.2.7.1. Compressor.

- The corrected volumetric flow *cmp*.
- The compression ratio $\pi^{cmp} = p_1/p_0$.
- The corrected revolutions N_c^{cmp}.
- The efficiency of the compressor η^{cmp}.

Given a point of the compressor map (g_c^{cmp}, π^{cmp}), it is possible to calculate:

- The composition x_1, $x_1 = x_0$.
- The compressor downstream pressure as: $p_1 = \pi^{cmp} p_0$.
- The compressor outlet temperature as a function of the isentropic evolution and the efficiency, T_1.
- The compressor power as: $\dot{W}^{cmp} = G^{cmp}(h_1 - h_0)$.

2.2.7.2. In-cylinder map. Using the thermodynamic mixed model to simulate the scavenging and combustion processes, it is possible to calculate:

- The inlet flow G^{adm}.
- The outlet flow G^{esc} and the composition x^{esc}.
- The exhaust temperature T^{esc}.

As a function of:

- The inlet conditions p_2 and T_2.

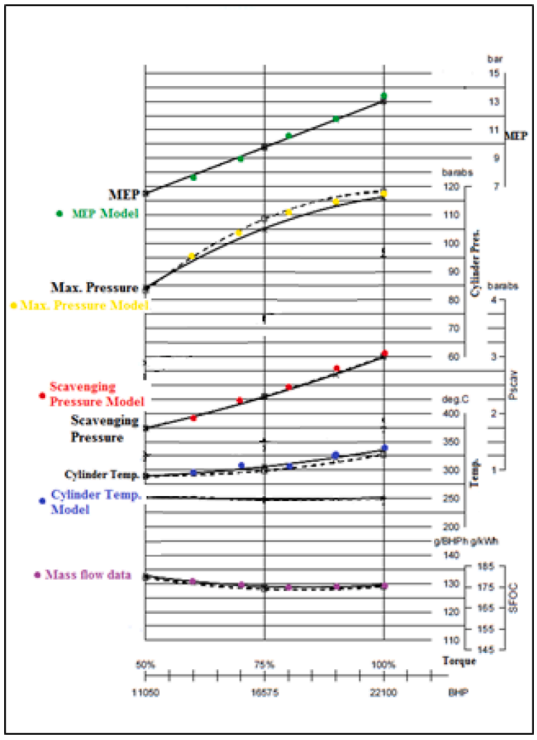

Fig. 8. Main magnitudes of the engine depending on the load and in colour the points obtained from the model for validation.

- The exhaust receiver pressure, p_3. $p_3 = \pi^p p_2$, where π^p is the relationship between the exhaust receiver pressure and the air receiver pressure.

Given a fuel mass injected (diesel and H_2), p_2, T_2 and π^p, we obtain G^{adm}, G^{esc}, x^{esc} and T^{esc}.

2.2.7.3. Turbine. The turbine is characterised by:

- A shape parameter β^{trb}.
- The corrected revolutions N_c^{trb}.
- The corrected mass flow G_c^{trb}.
- The expansion turbine ratio $\pi^{trb} = p_3/p_4$.
- The turbine efficiency η^{trb}.

Given a point of the turbine map (β^{trb}, N_c^{trb}), it is possible to calculate:

- The composition x_4, $x_3 = x_4$.
- The downstream pressure p_4, $p_4 = p_3/\pi^{trb}$.
- The turbine outlet temperature as a function of the isentropic expansion and the efficiency, T_4.
- The compressor power as: $\dot{W}^{trb} = G^{trb}(h_3 - h_4)$.

The matching process involves searching for the compressor map point (g_c^{cmp}, π^{cmp}), the ratio between the exhaust receiver pressure and the air receiver pressureπ^p, and the shape parameter of the turbine β^{trb}, that ensures:

$$\frac{G^{cmp}}{5G^{adm}} - 1 = 0 \tag{20}$$

$$\frac{G^{trb}}{5G^{adm}} - 1 = 0 \tag{21}$$

$$\frac{\pi^p p_2}{\pi^{trb} p_0} - 1 = 0 \tag{22}$$

$$\frac{\dot{W}^{cmp}}{\dot{W}^{trb}} - 1 = 0 \tag{23}$$

2.3. Model validation – Diesel mode

Fig. 7 shows the process that is carried out to develop the complete study, which is accounted in four steps. The first one, the blue block, corresponds to the development of the engine model. The second block in golden corresponds to the validation of the model in diesel mode from the pressure curves and operational data shown in Fig. 8 for different rated power levels (25–100%). The third block in red corresponds to the study of the operation of the 2 T engine model, previously validated, in dual mode with the addition of H_2 through the intake ports along with the air. Finally, in step 4 in green, different alternatives are studied for improving the engine performance.

The study of the effects of H_2 addition combined with WI on the in-cylinder pressure and temperature, the efficiency and MEP under various engine loads, water and H_2 fractions were carried out through numerical calculations using the 2 T engine model. Only the PHRRs have been obtained through previous experimentation, collected in references [24] and [25].

In Fig. 8, the black lines and points represent the current engine data and the different colour dots are the outputs from the model. As can be

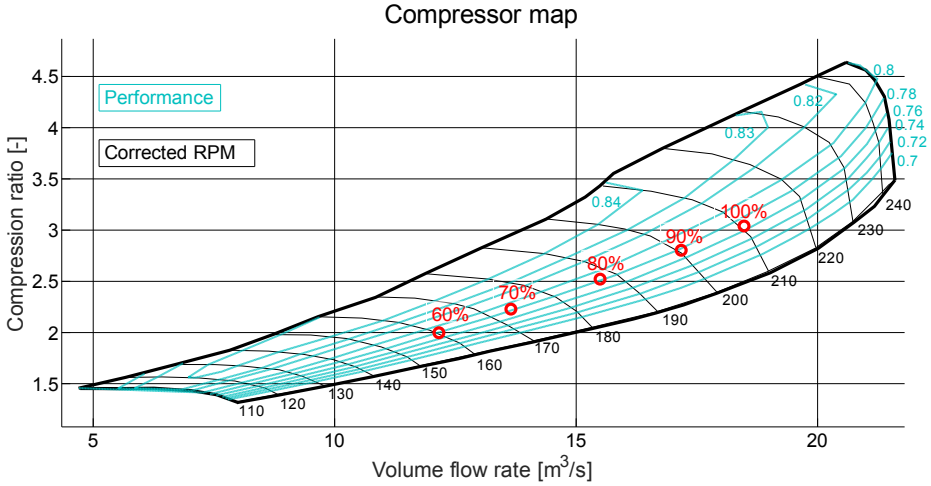

Fig. 9. Selected operating points to validate the 2 T engine model over the compressor map.

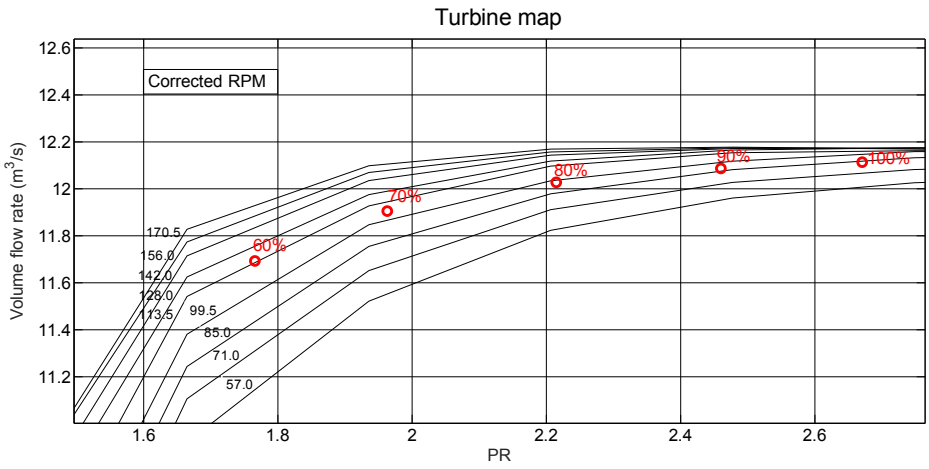

Fig. 10. Selected operating points to validate the 2 T engine model over the turbine map.

Table 3
Parameters of the PHRR for different energy fractions of the H_2.

Energy fraction of H_2	θ_0	θ_1	θ_2	m_1	m_2	A_1	A_2
0.00	2.00	3.00	8.0	2.50	1.00	0.200	0.800
0.25	6.89	4.18	7.63	2.58	0.688	0.082	0.949
0.50	4.00	10.23	22.65	1.61	2.63	0.856	0.184
0.80	6.73	5.01	9.23	2.91	1.35	0.144	0.932

observed, the model follows the engine performance with very low error.

For the development of the internal map of the cylinder, several iterations are required to achieve stationary conditions and to obtain a map point for the given conditions. To obtain the stationary conditions, the following steps are taken: for each new iteration the in-cylinder pressure curves are compared with the previous iteration, obtaining an error between them. If this error is less than a previously set value, the cylinder operating point is validated.

The MEP of the model depends on the mechanical losses introduced in the 2 T engine model, which has been adjusted so that the MEP adapts to the real curve, as shown in Fig. 7. Moreover, Fig. 9 and Fig. 10 show the selected operating points to validate the 2 T engine model in diesel mode over the compressor and turbine maps respectively.

Regarding calibration of the engine model with dual combustion HFO-hydrogen, currently there is no any engine of this type running with this fuel at any fuel mixture fraction and therefore it is not possible validation from operational data. In this regard, authors consider enough for the purpose of the work the validation of the engine model when runs in diesel mode. Therefore, the engine performance in dual combustion mode HFO-hydrogen presented in this work has to be considered as performance prediction.

3. Experimental study

3.1. Dual-fuel (diesel–hydrogen) operation

For the analysis of the dual mode, three load conditions have been selected: 100%, 80% and 60% of rated power in diesel mode, with different fractions of H_2 which are shown in Table 2. For every load condition, the energy of the mixture HFO-H_2 is the same of the corresponding energy of the diesel mode.

When required, water will be introduced with the intake air in the plenum, through injection close to the intake ports.

From the established load conditions and taking into account the mass ratio τ, the PHRR laws obtained [24,25] are incorporated into the model. The mass of water corresponding to the mass ratio is included in the model as well, named as μ in Table 2. The PHRRs taken are dimensionless, so that they are included in the model multiplied by the energy associated with the mass of fuel. Table 3 shows the value of the PHRR parameters [24,25].

Fig. 11 shows the different phases of the typical diesel combustion process in a PHRR curve. It can be observed that the combustion process contains a mixing-controlled phase and a diffusion phase.

From Fig. 12 (a) to (d) represents the Wiebe dimensionless PHRR

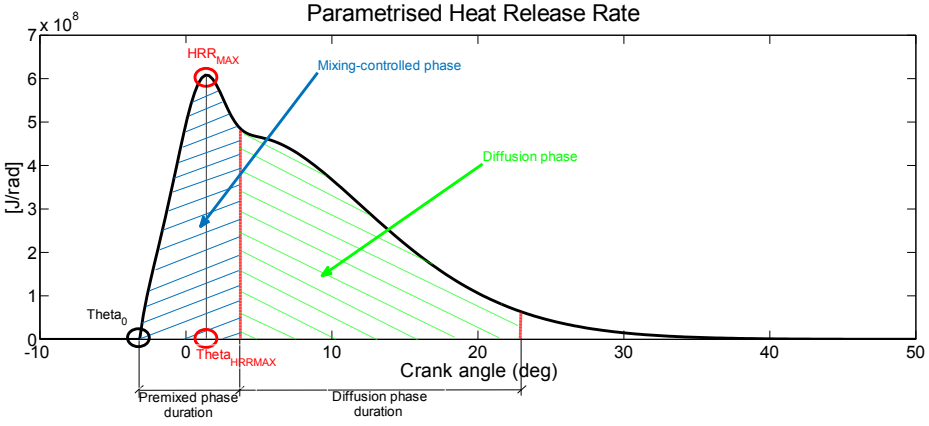

Fig. 11. Representation of the PHRR.

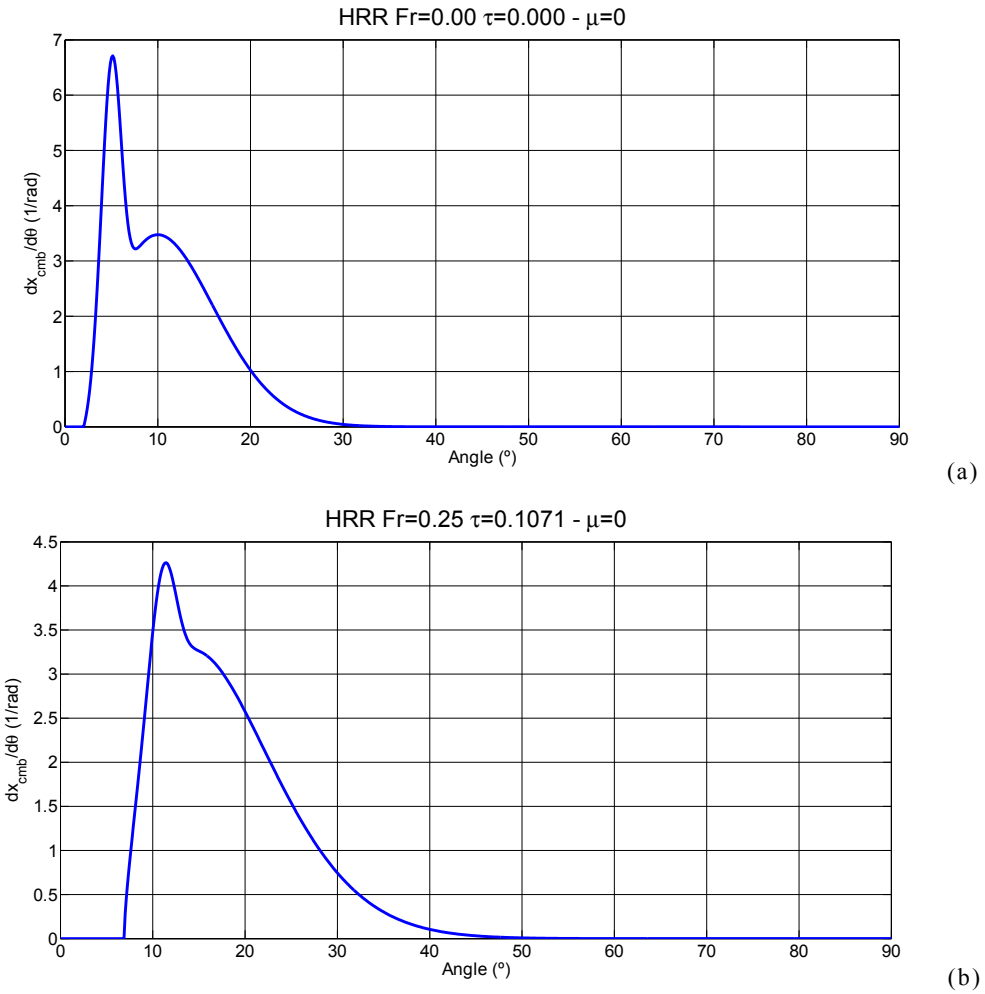

Fig. 12. PHRR for each energy fraction of H_2.

versus crank angle for each energy fraction of H_2 that corresponds to the parameters of Table 3. In Fig. 12 it can be observed that an increase in the H_2 energy fraction causes an evolution of the combustion process from a process with two phases (mixing-controlled and diffusion) to one with a single (mixing-controlled phase). This change in the HRR is due to the multiple turbulent flames propagated through the H_2–air mixture presented outside the diesel spray, accelerating the combustion process of the diesel fuel. The amount of H_2O has no influence on the shape of the PHRR. Analysing the role of the WI in the PHRR, a delay is observed in the start of combustion as WI increases.

Fig. 13 shows the compressor map for the different fractions of H_2 introduced; as it is shown, both the air mass flow and the compression ratio decrease proportionally to the increase of H_2 involved in the process. Table 4 shows the reduction of MEP and air mass flow in dual mode operation. Keeping the exhaust valve open at the same time as the intake ports causes H_2 leaks in the scavenging process before it can be burned, less power by cylinder and a lower exhaust temperature, providing less energy at the turbine inlet. This promotes a reduction of the turbocharger speed and therefore of the pressure and air mass flow when compared to the case of 0% H_2.

Fig. 13 and the next figures on the map of the compressor and the turbine show 100%, 80% and 60% of rated power indicated with boxes.

In order to correct the power reduction due to the loss of mass of H_2 through the exhaust valve, two solutions are proposed:

(1) An earlier exhaust valve closure so that the amount of H_2 that leaves the cylinder without burning is reduced, mainly due to the lower time for H_2 leakages. This solution does not require any additional modification to the original engine and its implementation in the real engine is immediate by adjusting the opening cam.
(2) Injecting the H_2 when the exhaust valve has closed. In this case there is no possibility of H_2 leakage with exhaust gases. To carry out this modification, an injector is required to introduce the H_2 directly into the chamber. From a technical point of view, this solution is easy to implement due to the high pressure in the H_2 tank, in the range 300–700 bar, and the low pressure in the cylinder after exhaust valve closure, lower than 40 bar.

3.2. New engine configuration for improving performance

3.2.1. An earlier exhaust valve closure

Figs. 14 and 15 show the following cases on the compressor map, with the main engine outputs presented in Table 4:

- Cases in diesel reference mode and with the exhaust valve closing according to the normal distribution. They are shown with the symbol “x”.
- Case of the normal exhaust valve closure distribution, + 92° after BDC. This case is represented by circle of different colours, one for each different fraction of H_2.

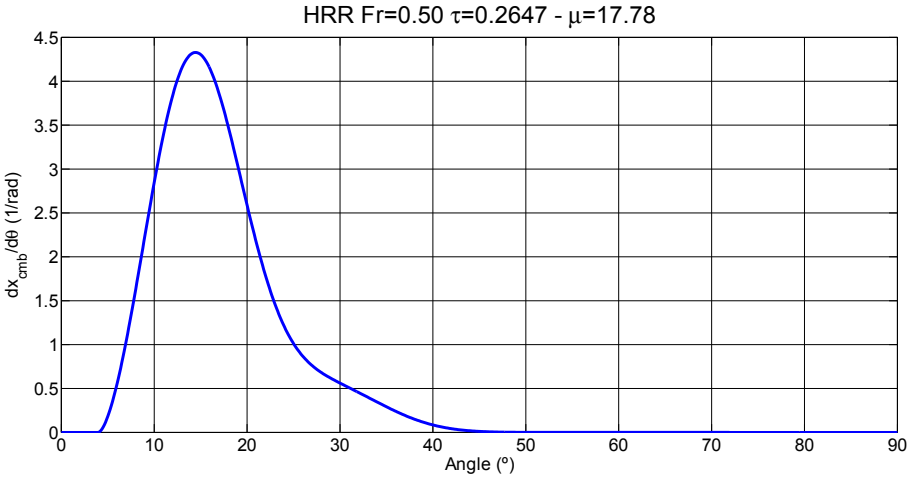

(c)

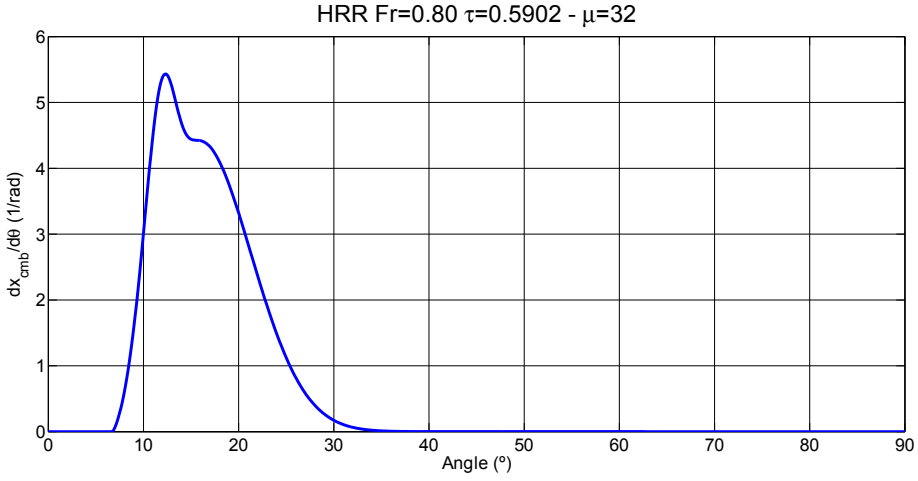

(d)

Fig. 12. (*continued*).

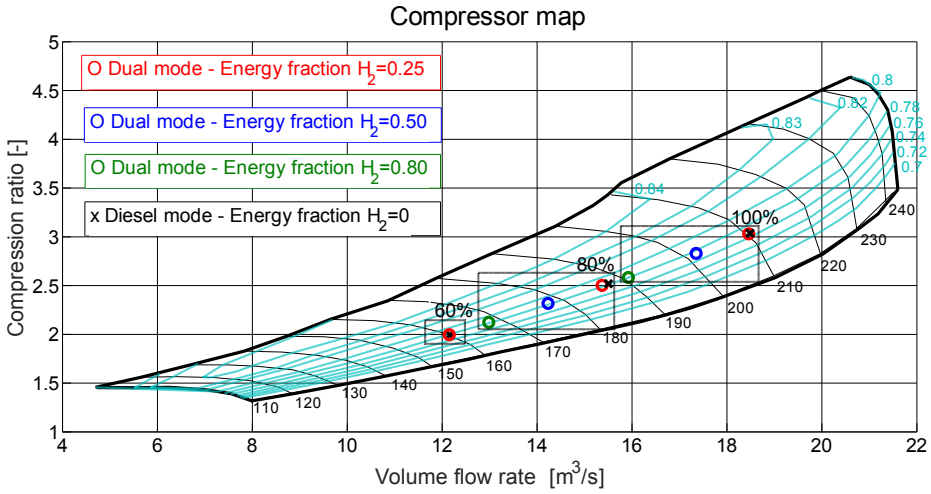

Fig. 13. Operating points in dual-fuel mode over the compressor map.

- Case of advance closing of the exhaust valve, 30° before normal distribution. That is to say, the closing takes place +60° after BDC. Represented by squares of different colours.
- Case of advance closing of the exhaust valve, 50° before normal distribution. That is to say, the closing takes place +40° after BDC. Represented by asterisks of different colours.
- Case of advance closing of the exhaust valve, 65° before normal distribution. In this case, closing is +25° after BDC. Represented by asterisks of different colours.

Figs. 16, 17 and 18 show the variation of the MEP, the admission flow and the performance for different exhaust valve closing angles. For

Table 4
Comparison of the values obtained in the dual mode model for the proposed solutions to prevent H_2 leakage.

	Energy fraction H_2	Rated power	MEP (bar)	Intake flow (kg/h)	Losses of H_2	Efficiency
Diesel Mode	0	100%	13.51	8.70	–	49.13
		80%	10.52	7.30	–	47.83
		60%	7.64	5.72	–	46.31
Dual Mode - EVC + 92° after BDC	0.25	100%	13.17	8.68	35%	47.90
		80%	10.54	7.24	35%	47.92
		60%	7.44	5.72	32%	45.10
	0.50	100%	12.05	8.16	36%	43.82
		80%	9.59	6.70	35%	43.60
	0.80	100%	10.74	7.50	37%	39.06
		80%	8.65	6.12	36%	39.32
Dual Mode - EVC + 60° after BDC	0.25	100%	13.50	8.70	22%	49.10
		80%	10.70	7.30	22%	48.64
		60%	7.72	5.67	20%	46.79
	0.50	100%	13.15	8.40	23%	47.83
		80%	10.55	6.94	22%	47.96
	0.80	100%	12.54	8.14	24%	45.61
		80%	10.02	6.74	23%	45.55
Dual Mode - EVC + 40° after BDC	0.25	100%	13.41	8.55	15%	48.77
		80%	10.53	7.16	14%	47.87
		60%	7.85	5.46	13%	47.58
	0.50	100%	13.09	8.46	15%	47.61
		80%	10.29	6.90	15%	46.78
		60%	7.71	5.29	13%	46.73
	0.80	100%	12.88	8.31	16%	46.84
		80%	10.17	6.76	15%	46.23
Dual Mode - EVC + 25° after BDC	0.25	100%	13.41	8.31	10%	48.77
		80%	10.51	6.72	10%	47.78
	0.50	100%	13.22	8.22	11%	48.08
		80%	10.38	6.60	10%	47.19
	0.80	100%	13.23	8.23	11%	48.12
		80%	10.42	6.23	10%	47.37
Dual Mode – H_2 Injection	0.25	100%	13.81	8.99	–	50.23
		80%	10.85	7.69	–	49.33
		60%	8.09	6.09	–	49.04
	0.50	100%	14.05	9.04	–	51.10
		80%	11.05	7.71	–	50.23
		60%	8.24	6.19	–	49.95
	0.80	100%	14.62	9.21	–	53.17
		80%	11.50	7.87	–	52.28
		60%	8.59	6.26	–	52.07

all figures, the legend indicates that an "x" symbol, a "□" symbol and a "▲" symbol correspond to 100%, 80% and 60% of rated power, respectively. The different colors of the figures refer to the closing angle of the exhaust valve, in this case the red, blue, green and yellow colors corresponding to +92° (normal closing of the valve), +60°, +40° and +25°, all after BDC, respectively.

It can be appreciated that closing the exhaust valve earlier produces an increase in the MEP and efficiency; the higher the H_2 fraction, the earlier the exhaust valve closing required for performance improvement. It is also observed that the earlier the exhaust valve closing, the higher the mass flow reduction. In dual mode, closing the exhaust valve 25° before BDC gives only a small reduction of performance when compared to the original engine burning HFO.

Fig. 14 shows another effect of the earlier exhaust valve closing; as the exhaust valve closing angle moves towards BDC, the operating points approach the compressor's pumping line. This behaviour is due to the fact that advancing the closing of the exhaust valve means that the compressor has a higher back pressure accompanied by a reduction of the compressor flow. In addition and because the amount of fuel is maintained, there is an increase of the fuel–air equivalence ratio increasing the exhaust gases temperature, see Fig. 19, and pressure ratio, see Fig. 15, where the PR ratio increases as the exhaust valve closing is nearer to the BDC.

Fig. 20 shows the in-cylinder pressure curve at 100% of rated power for different angles of exhaust valve closing as a function of the energy fraction of H_2. For the same exhaust valve opening angle, any increase of H_2 reduces the pressure at TDC, because of the reduction of compressor pressure and also reduces the maximum combustion pressure due to the increasing leakage of hydrogen. On the contrary, an earlier exhaust valve closure causes an increase in the compression pressure at TDC and also of the maximum combustion pressure for both the increase of air pressure at inlet port closure and the increase of H_2 ratio (upward movement of the pressure curves).

3.2.2. H_2 direct injection

Figs. 21 to 27 show the output of the engine when H_2 injection is after exhaust valve closure, inhibiting any H_2 leakage into the exhaust flow. The engine outputs performance is summarised in Table 4. For these figures the following legend has been adopted:

- Diesel mode reference with the exhaust valve closing at +92° after BDC. This is shown with the symbol "x".
- Dual-fuel mode (without injection of H_2) with the exhaust valve closing at +92° after BDC. This case is represented by circles of different colours, this is, different fractions of H_2.

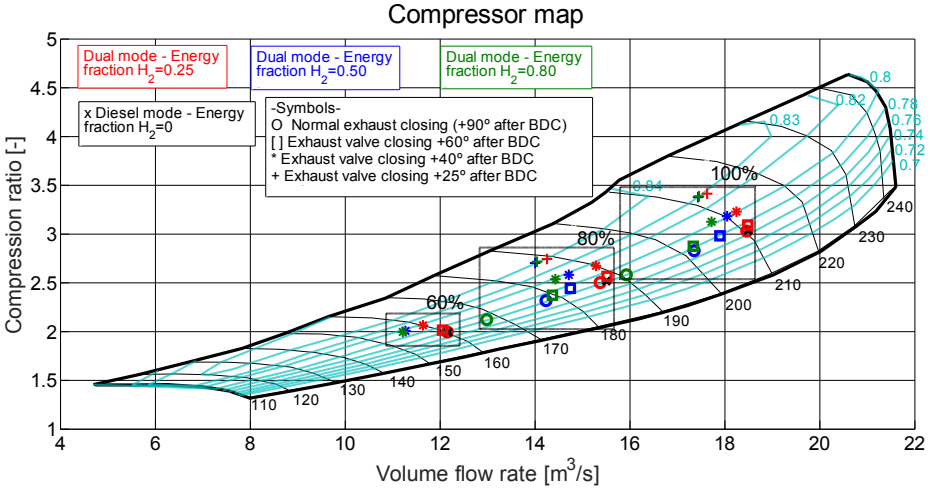

Fig. 14. Compressor map with the operating points with different exhaust valve closure.

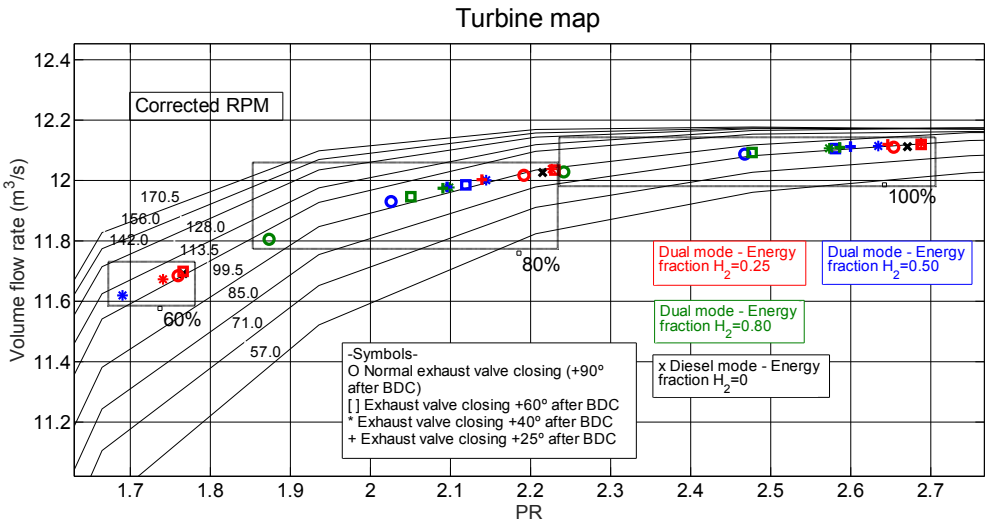

Fig. 15. Turbine map with the operating points with different exhaust valve closure.

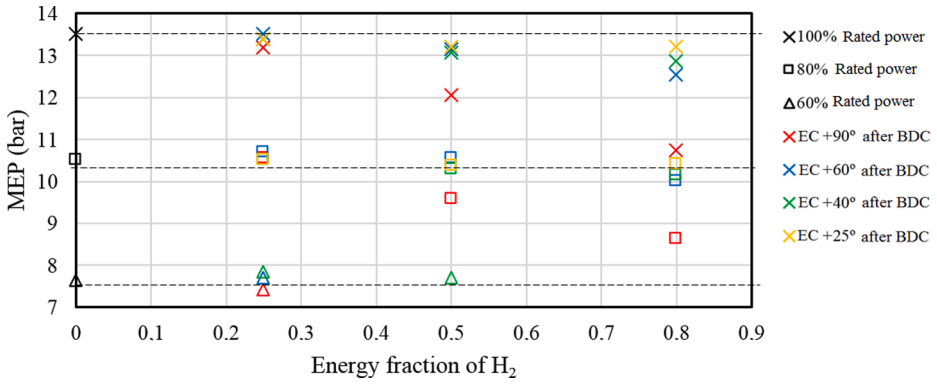

Fig. 16. Comparison in terms of MEP between the different cases of exhaust valve closure.

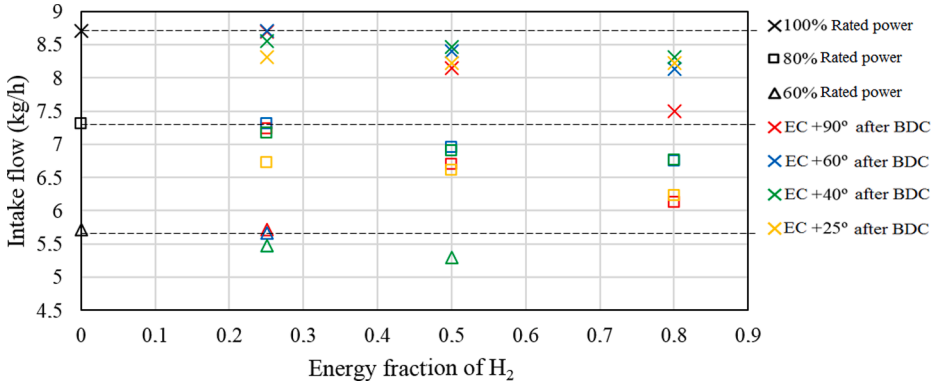

Fig. 17. Comparison in terms of intake flow between the different cases of exhaust valve closure.

- Dual-fuel mode with H_2 injection. This case is represented by squares of different colours, this is, different fractions of H_2.

In Fig. 22, the case with the exhaust valve closing at +25° after BDC and H_2 at intake is included to compare the results with the H_2 injection case. It is observed in Fig. 21 that the operating points in which H_2 has been injected have a greater volume flow rate, increasing the compression ratio. This behaviour is produced by two different phenomena:

- The fresh air after the compressor is not displaced by hydrogen at the inlet and consequently there is a lower H_2/air ratio when compared with the cases before. As a result, the exhaust temperature will be lower in the injection mode, as can be observed in Fig. 23.
- The reduction of the back pressure when the exhaust valve is closed at +92° after BDC, together with a slight increase in the available energy in the exhaust because the entire quantity of H_2 is burned, except that associated with the combustion efficiency.

Fig. 24 shows the operating points on the turbine map. It can be

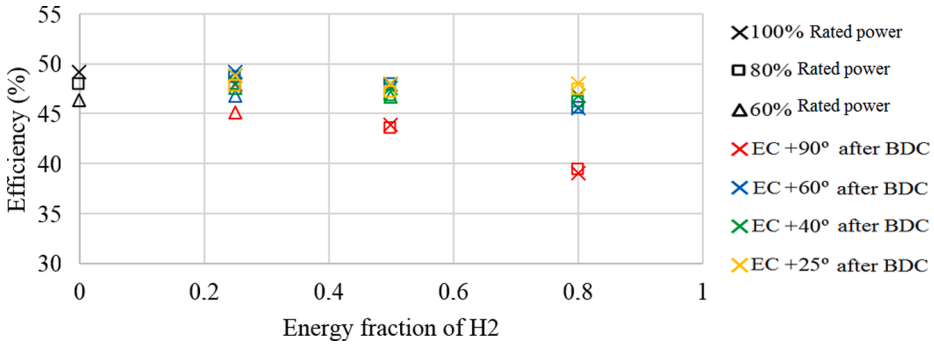

Fig. 18. Comparison in terms of efficiency between the different cases of exhaust valve closure.

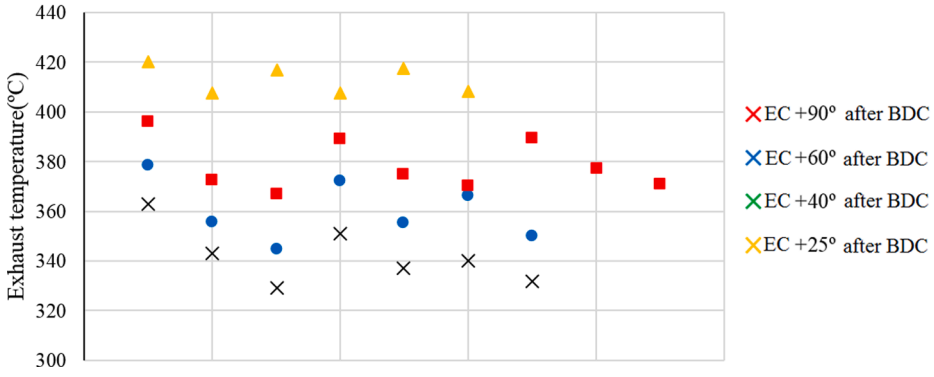

Fig. 19. Comparison in terms of exhaust temperature between the different cases of exhaust valve closure.

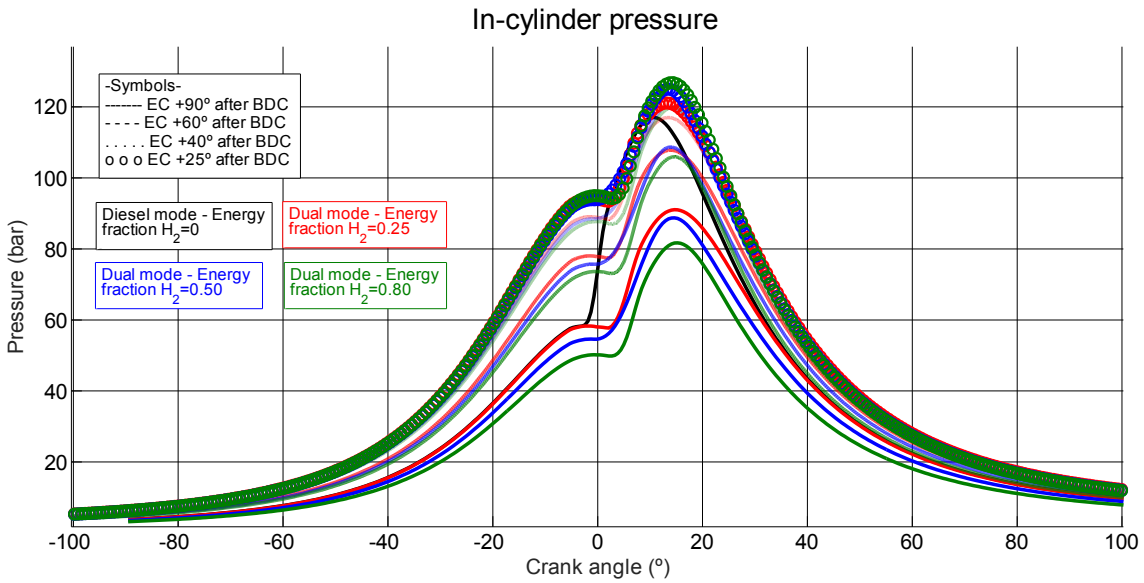

Fig. 20. In-cylinder pressure curves at 100% of rated power for different cases of exhaust valve closure.

observed that, as the compression ratio in the compressor increases, the PR ratio in the turbine also increases.

Fig. 25 shows the efficiency for the following cases: the reference case (diesel mode), the dual mode operation with H_2 injection and the case of dual mode operation with the contribution of H_2 through the intake ports with the closure of the exhaust valve at +92° after the BDC. It can be seen in the figure that H_2 injection after exhaust valve closure represents an improvement in performance with respect to the other cases. This effect is greater when the energy fraction of H_2 grows. The best results are obtained for an energy fraction of 0.80.

Fig. 26 shows the MEP for the reference case and the case of dual mode operation with H_2 direct injection. As with the performance, a higher energy fraction of H_2 produces a greater increase in MEP. This is due to the fact that combustion is faster, approaching a constant volume process, which results in an increase in MEP.

Fig. 27 shows the in-cylinder pressure for the rated power equal to 100% for cases of operation in diesel mode, dual operation mode with exhaust closure at +90° after BDC, dual operation mode with exhaust

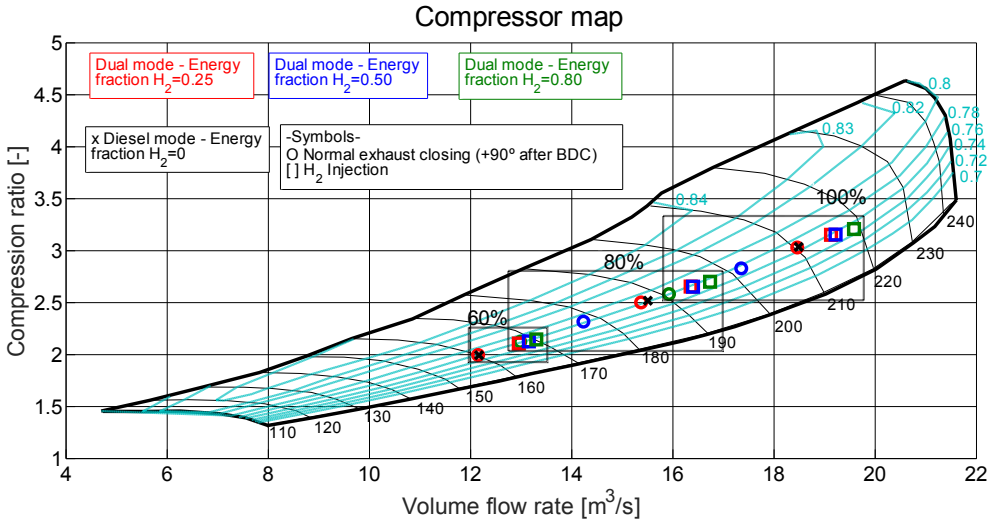

Fig. 21. Compressor map with the operating points with H_2 direct injection and exhaust valve closure at +92° after BDC.

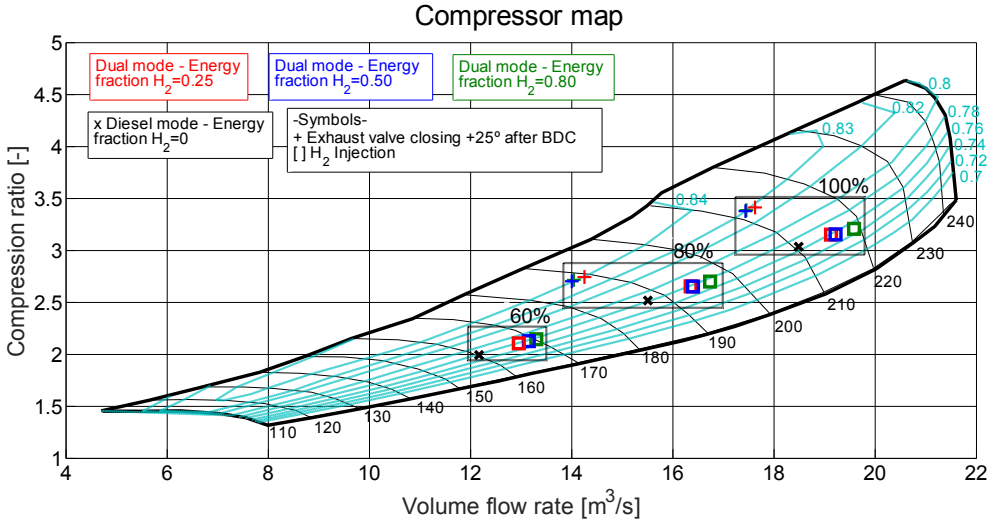

Fig. 22. Compressor map with the operating points with H_2 direct injection and exhaust valve closure at +25° after BDC.

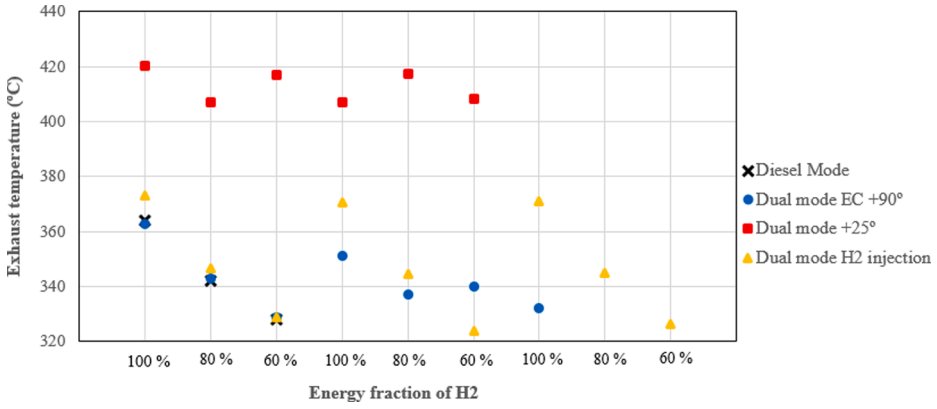

Fig. 23. Comparison in terms of exhaust temperature for different cases.

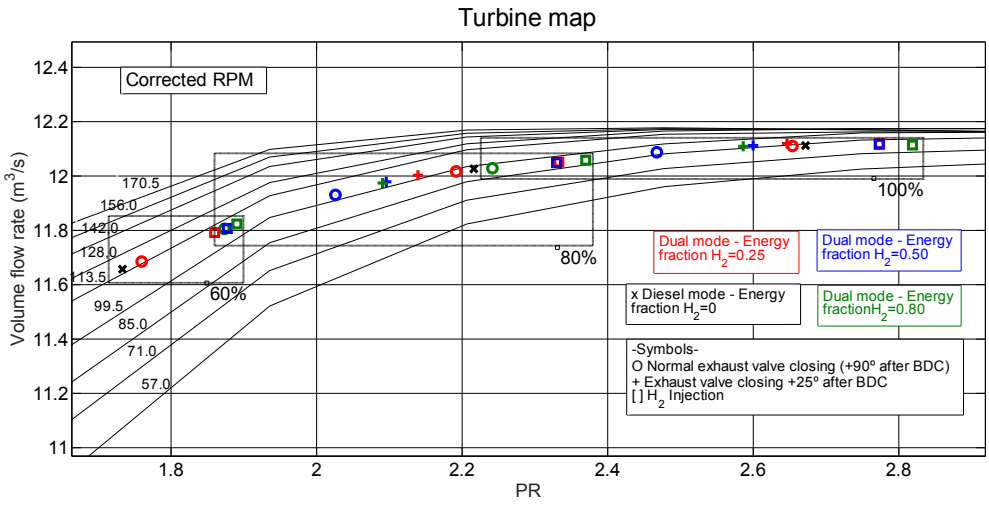

Fig. 24. Turbine map with the operating points with H_2 direct injection and exhaust valve closure at +92° after BDC.

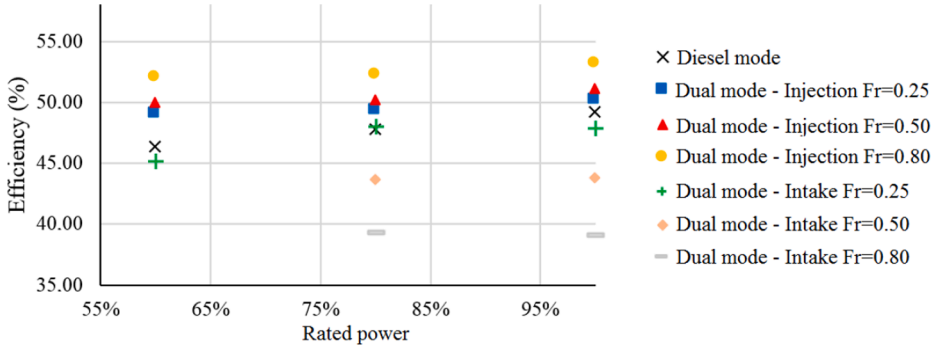

Fig. 25. Comparison in terms of efficiency for different cases.

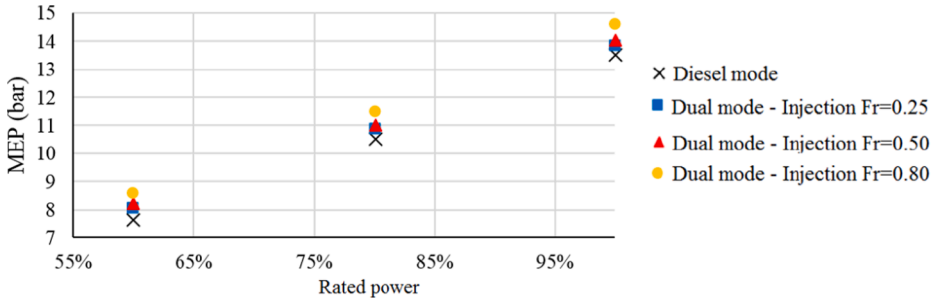

Fig. 26. Comparison in terms of MEP for different cases.

closure at +25° after BDC and dual operation mode with H_2 direct injection for different H_2 fractions. Comparison with Fig. 19 shows that the maximum combustion pressure with H_2 injection does not increase and therefore the increases of MEP and efficiency do not compromise the mechanical integrity of the engine.

Table 4 shows a comparison of the values obtained in the dual mode model for the proposed solutions to prevent H_2 leakage.

Although the thermodynamic model is not able to provide NOx and particulate emissions data, based on the previous experimental study on the conventional diesel engine and observing the reduction in the fuel air equivalence ratio with H_2 injection, it is expected that these emissions will be reduced as the energy fraction of H_2 grows. This is because, on the one hand, the contribution of fossil fuels is reduced, reducing the emissions of CO_2, CO and particles; and on the other hand, the contribution of H_2O has been implemented in the model with the benefits that we have observed in the previous experimental study on the conventional diesel engine [24,25].

4. Conclusions

This paper presents a methodology to analyse the effects of using H_2 as fuel in a 2 T low-speed diesel engine. The engine performance has been studied under various test conditions, and the conclusions drawn from this investigation are as follows:

- The thermodynamic model developed for the 2 T diesel engine fits closely current engine performance, and is thus a sound tool for studying alternative solutions to burning HFO.

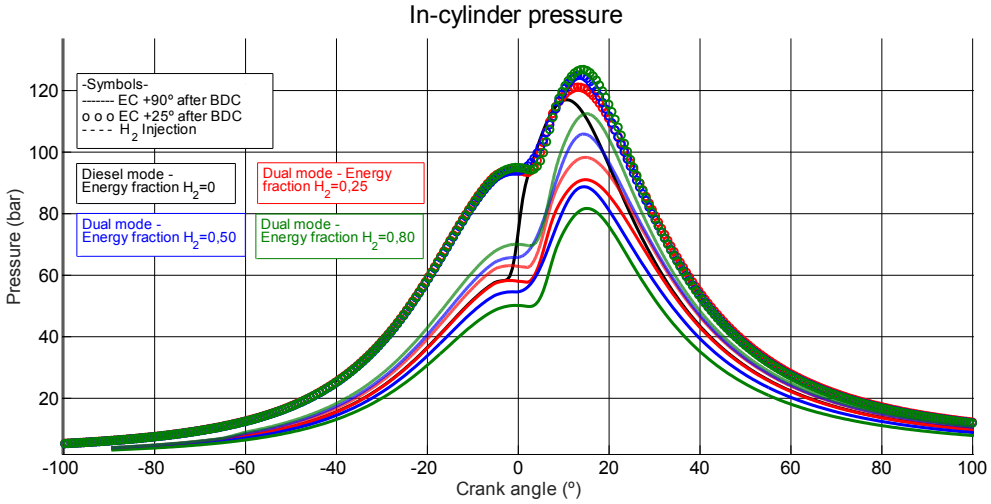

Fig. 27. In-cylinder pressure curves at 100% of rated power for different cases.

• The use of H2 as fuel in a low-speed two-stroke diesel engine combined with water injection is feasible and presents results that match or improve the performances of the engine in diesel combustion mode. Therefore, hydrogen can be considered a sound candidate as green fuel (when comes from renewable energy) for power production and naval propulsion with the most efficient 2-stroke engines.

- Due to the characteristics of this type of engine, part of the H_2 supplied would be lost during the scavenging and therefore engine performance would be reduced. Two strategies have been proposed to improve performances that have shown their validity: 1) an earlier exhaust valve closure and 2) injecting the H2 when the exhaust valve has closed.
- In the case of H_2 supply with the intake air, it is necessary to advance the exhaust valve closing angle to reduce hydrogen leakage with exhaust gases. With a reduction of 65° of the closure angle, the engine performance experiences a very small power and efficiency penalty, almost null. The MEP when closing the exhaust valve 25° after BDC is around 0.1 bar lower than in the case of operation in diesel mode. The best result is 13.41 bar and 49% of efficiency at 100% of rated power.
- H_2 injection can improve the current high efficiency of a 2 T diesel engine burning HFO, achieving more than 53%. This figure suggests a feasible alternative to FC or other less polluting technologies that would still be far from being competitive for high output power. The performance improvements do not increase the peak combustion pressure and therefore minor changes are required for adapting current 2 T engines for burning H_2.
- Considering the current use of these 2 T diesel engines burning HFO, changing to dual combustion mode with H_2 injection will reduce CO_2 emissions by roughly 0.78 tons /MWh at full power. For a typical mean engine use of 7000 h/year at 80% of nominal engine load for the engine of Table 1, changing HFO to dual combustion mode with H2 injection will reduce the CO_2 roughly by 70 tons/year.

CRediT authorship contribution statement

J. Serrano: Software, Formal analysis, Investigation, Data curation, Writing - review & editing, Visualization. **F.J. Jiménez-Espadafor:** Conceptualization, Methodology, Investigation, Supervision, Project administration, Funding acquisition. **A. López:** Software, Formal analysis, Data curation.

Declaration of Competing Interest

The authors declare that they have no known competing financial interests or personal relationships that could have appeared to influence the work reported in this paper.

Acknowledgements

This work was supported by the Junta de Andalucía (Consejería de Economía, Conocimiento, Empresas y Universidad) as part of item AT17_5934_US within the Plan Andaluz de Investigación, Desarrollo e Innovación (PAIDI 2020), Andalucía-Spain.

Authors are also very grateful to the support of Endesa Soporte-Técnico Motores Diesel in the development of this work, mainly to Mr. Fco. Fernández Vacas.

References

[1] Emission Control MAN B&W Two-stroke Diesel Engines. http://www.flamemarine.com/files/MANBW.pdf [accessed 08 January 2020].
[2] D. Palomo Guerrero, F. Jimenez-Espadafor Aguilar, Torsional system dynamics of low speed diesel engines based on instantaneous torque: Application to engine diagnosis, Mech. Syst. Sig. Process. 116 (2019) 858–878.
[3] Doug Woodyard, Pounder's Marine Diesel Engines, Exhaust emissions and control, 8th Edition. Butterworth-Heinemann, 2004 https://doi.org/10.1016/B978-075065846-1/50004-3.
[4] International Maritime Organization, Third IMO greenhouse gas study 2014, International Maritime Organization, London, 2014. http://www.imo.org/en/OurWork/Environment/PollutionPrevention/AirPollution/Documents/Third%20Greenhouse%20Gas%20Study/GHG3%20Executive%20Summary%20and%20Report.pdf [accessed 27 April 2020].
[5] T.W.P. Smith, J.P. Jalkanen, B.A. Anderson, J.J. Corbett, J. Faber, S. Hanayama, et al., Third IMO GHG study 2014. Tech. rep., International Maritime Organization (IMO), London, UK, 2015.
[6] Batteries on board ocean-going vessels, https://marine.man-es.com/docs/libraries provider6/test/batteries-on-board-ocean-going-vessels.pdf?sfvrsn=9c69d8a2_4 [accessed 08 January 2020].
[7] MAN Diesel & Turbo, Tier III two-stroke technology, Technical Paper, 2012. http://marine.man.eu/two-stroke/technical-papers [accessed 08 January 2020].
[8] Y. Ryu, Y. Lee, J. Nam, Performance and emission characteristics of additives-enhanced heavy fuel oil in large two-stroke marine diesel engine, Fuel (2016), https://doi.org/10.1016/j.fuel.2016.06.029.
[9] Ballard blog. Fuel-cells-marine-vessels. https://blog.ballard.com/fuel-cells-marine-vessels [accessed 08 January 2020].
[10] L. Van Biert, M. Godjevac, K. Visser, P.V. Aravind, A review of fuel cell systems for maritime applications, J. Power Sources 327 (2016) 345–364, https://doi.org/10.1016/j.jpowsour.2016.07.007.
[11] Yusuf Bicer, Ibrahim Dincer, Environmental impact categories of hydrogen and ammonia driven transoceanic maritime vehicles: A comparative evaluation, Int. J. Hydrogen Energy 43 (2018) 4583–4596, https://doi.org/10.1016/j.ijhydene.2017.07.110.

[12] Konstantinos Kakosimos, Hertel Ole, Ketzel Matthias, R. Berkowicz, Operational street pollution model (OSPM) e a review of performed application and validation studies and future prospects, Environ. Chem. 7 (6) (2010), 485e503.
[13] I.P. Jain, Hydrogen the fuel for 21st century, Int. J. Hydrogen Energy 34 (2009) 7368–7378, https://doi.org/10.1016/j.ijhydene.2009.05.093.
[14] V. Chintala, K.A. Subramanian, Experimental investigation of hydrogen energy share improvement in a compression ignition engine using water injection and compression ratio reduction, Energy Convers. Manage. 108 (2016) 106–119, https://doi.org/10.1016/j.enconman.2015.10.069.
[15] S. Nag, P. Sharma, A. Gupta, Dhar, Combustion, vibration and noise analysis of hydrogen-diesel dual fuelled engine, Fuel 141 (2019) 488–494. https://doi.org/10.1016/j.fuel.2018.12.055.
[16] Vinod Singh Yadav, S.L. Soni, Dilip Sharma, Engine performance of optimized hydrogen-fueled direct injection engine, Energy 65 (2014) 116–122, https://doi.org/10.1016/j.energy.2013.12.007.
[17] Madan Kumar, Taku Tsujimura, Yasumasa Suzuki, NOx model development and validation with diesel and hydrogen/diesel dual-fuel system on diesel engine, Energy 145 (2018) 496–506, https://doi.org/10.1016/j.energy.2017.12.148.
[18] Midhat Talibi, Paul Hellier, Robert Morgan, Chris Lenartowicz, Nicos Ladommatos, Hydrogen-diesel fuel co-combustion strategies in light duty and heavy duty CI engines, Int. J. Hydrogen Energy 43 (2018) 9046–9058, https://doi.org/10.1016/j.ijhydene.2018.03.176.
[19] M. Talibi, Co-combustion of diesel and gaseous fuels with exhaust emissions analysis and in-cylinder gas sampling, PhD Thesis (Doctoral), University College London, 2015.
[20] Lijun Wang, Dong Liu, Zhenzhong Yang, Hailin Li, Leyu Wei, Quancai Li, Effect of H2 addition on combustion and exhaust emissions in a heavy-duty diesel engine with EGR, Int. J. Hydrogen Energy 43 (2018) 22658–22668. https://doi.org/10.1016/j.ijhydene.2018.10.104.
[21] E. Monemian, A. Cairns, M. Gilmore, D. Newman, K. Scott, Evaluation of intake charge hydrogen enrichment in a heavy-duty diesel engine, Proc. Instit. Mech. Eng., Part D: J. Automobile Eng. 232 (1) (2018) 139–147, https://doi.org/10.1177/0954407017738375.
[22] Horng-Wen Wu, Tzu-Ting Hsu, Jian-Yi He, Chen-Ming Fan, Optimal performance and emissions of diesel/hydrogen-rich gas engine varying intake air temperature and EGR ratio, Appl. Therm. Eng. 124 (2017) 381–392, https://doi.org/10.1016/j.applthermaleng.2017.06.026.
[23] J. Serrano, F.J. Jiménez-Espadafor, A. Lora, L. Modesto-López, A. Gañán-Calvo, J. López-Serrano, Experimental analysis of NOx reduction through water addition and comparison with exhaust gas recycling, Energy 168 (2019) 737–752, https://doi.org/10.1016/j.energy.2018.11.136.
[24] J. Serrano, F.J. Jiménez-Espadafor, A. López, Analysis of the effect of different hydrogen/diesel ratios on the performance and emissions of a modified compression ignition engine under dual-fuel mode with water injection. Hydrogen-diesel dual-fuel mode, Energy 172 (2019) 702–711, https://doi.org/10.1016/j.energy.2019.02.027.
[25] J. Serrano, F.J. Jiménez-Espadafor, A. López, Analysis of the effect of the hydrogen as main fuel on the performance of a modified compression ignition engine with water injection, Energy. 173 (2019) 911–925, https://doi.org/10.1016/j.energy.2019.02.116.
[26] MAN B&W Diesel, Various internal material from man b&w diesel, 2005.
[27] J.B. Heywood, Internal Combustion Engines Fundamentals, McGraw-Hill, Inc., New York, 1988.
[28] W.J.D. Annand, Heat transfer in the cylinders of reciprocating internal combustion engines, Proc. Instit. Mech. Eng. 177 (1963) 973–996, https://doi.org/10.1243/pime_proc_1963_177_069_02.
[29] Payri Francisco, Olmeda Pablo, Martín Jaime, Antonio Garcia, A complete 0D thermodynamic predictive model for direct injection diesel engines, Appl. Energy 88 (2011) 4632e41. https://doi.org/10.1016/j.apenergy.2011.06.005.